Bicrystalline ZnS Microbelts

ARTICLE *in* CRYSTAL GROWTH & DESIGN · JUNE 2009

Impact Factor: 4.89 · DOI: 10.1021/cg9000363

6 AUTHORS, INCLUDING:

Baodan Liu
Chinese Academy of Sciences
89 PUBLICATIONS **2,073** CITATIONS
SEE PROFILE

Meiyong Liao
National Institute for Materials Science
131 PUBLICATIONS **3,668** CITATIONS
SEE PROFILE

Dmitri Golberg
National Institute for Materials Science
646 PUBLICATIONS **22,786** CITATIONS
SEE PROFILE

CRYSTAL GROWTH & DESIGN
2009
VOL. 9, NO. 6
2790–2793

Bicrystalline ZnS Microbelts

Baodan Liu,*,† Yoshio Bando,† Meiyong Liao,‡ Chengchun Tang,† Masanori Mitome,† and Dmitri Golberg†

WPI Center for Materials Nanoarchitectonics (MANA), and Sensor Materials Center, National Institute for Materials Science (NIMS), Namiki 1-1, Tsukuba, Ibaraki 305-0044, Japan

Received January 13, 2009; Revised Manuscript Received March 18, 2009

ABSTRACT: Bicrystalline ZnS microbelts with unusual structures were synthesized using chemical vapor deposition while adding MnO_2 into standard ZnS precursor. High-resolution transmission electron microscopy (HRTEM) and electron diffraction (ED) analyses showed that two neighboring crystals within each bicrystal are composed of $(0\bar{1}2)/(103)$ and $(010)/(103)$ planes with only one atomic layer of the (103) plane at the twin boundary, different from all previously reported ZnS twinned structures. UV sensors prepared from novel ZnS microbelts exhibited an ultrafast response and a decent stability under continuous UV irradiation, revealing a large promise for applications in nanoscaled UV-sensors.

Introduction

A bicrystal, different from periodically twinned solids, is composed of two well-defined mirror domains symmetrically located on both sides of the central axial twin boundary. Such crystals have frequently been observed in various nanostructures made of GaN, ZnO, Cu, etc.[1−3] Formation of bicrystalline nanostructures is mainly related to some critical growth conditions, for example, temperature fluctuations[1] or spatially separated changeable chemical environments.[4] These resulted in the metastable state appearance. Because of structural peculiarities, bicrystals have a large potential in specific applications, for example, in YBCO high-temperature superconductor (HTS) Josephson junctions.[5]

Zinc sulfide (ZnS), an important wide-bandgap semiconductor, possesses two distinct structures, namely, the wurtzite-type hexagonal structure with a stacking sequence of ABAB... along the [0001] direction and the zinc-blende-type cubic structure with a stacking sequence of ABCABC... along the [111] direction. Typically, the periodic twinned structures have been formed in zinc-blende-type ZnS with a (111) facet as the twin plane,[6] whereas the bicrystals were preferably observed in wurtzite-type ZnS.[7−9] So far, bicrystalline ZnS nanostructures composed of (001)/(013) or (012)/ (013) planes have been reported.[7,9] In this article, we discovered new bicrystalline structures in wurtzite-type ZnS microbelts, which consist of a (013) plane as the twin boundary and a pair of $(0\bar{1}2)$ or (010) planes.

Experimental Section

The bicrystalline ZnS microbelts were synthesized in a vertical induction furnace through a fully controlled chemical vapor deposition (CVD) process. A detailed experimental setup for the ZnS microbelt growth is illustrated in Supporting Information, Figure SI-1. High-purity ZnS and MnO_2 powders (Wako Chemical Co. Ltd.; purity 99.99%) were used as the precursors. A MnO_2 powder (∼5 wt %) was used as an additional agent, rather than as a dopant. Well-mixed ZnS and MnO_2 powders were loaded into a cylindrical Al_2O_3 crucible and then inserted into a vertical graphite inductor with a thin BN pipe inside it for preventing impurity invasion. A piece of Si (15 × 15) wafer coated with a thin Au layer was placed on the gas outlet, at the top of the synthetic chamber, for the deposition of ZnS microbelts. The reaction chamber was then quickly heated to 1300 °C in 10 min under an Ar flow (1.0 L/min). After reacting at 1300 °C for 30 min, the reaction system was cooled to room temperature under the protection of Ar gas. A large amount of fiber-like ZnS microbelts was found deposited on the Si substrate. The phase and purity of as-grown ZnS microbelts were examined by an X-ray powder diffractometer (XRD, Rigaku RINT 2000) operating at 40 kV and 40 mA, using Cu Kα radiation (λ = 1.54056 Å). The morphology characterization and structure analysis were carried out using a scanning electron microscope (SEM, JEOL, JEM-6700F) and a 300 kV high-resolution field-emission transmission electron microscope (TEM, JEOL, JEM-3000F). The composition analysis was performed by an energy dispersive X-ray spectometer (EDS) attached to the TEM. The ZnS UV sensor fabrication was carried out in a clean room using a multistep process, which included mask alignment (for defining the electrode patterns) and electron beam deposition of the Ti/Au electrodes. The photoresponse measurements were conducted at ambient pressure. An ultraviolet (UV)-enhanced Si photodiode with a wavelength of 320 nm was used as the irradiation source.

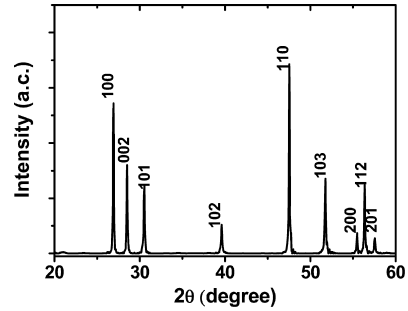

Figure 1. XRD pattern of bicrystalline ZnS microbelts grown on a Si substrate.

Results and Discussion

To check the phase purity of ZnS microbelts, XRD measurements were first carried out. Figure 1 shows an XRD pattern of bicrystalline ZnS microbelts. The belts are single-phase. All peaks can be perfectly indexed to a wurtzite-type ZnS of the P_{63mc} space group with the lattice constants a = 3.818 Å, and c=6.26 Å, (JCPDS card no. 89-2942). This indicates that adding MnO_2 powders does not lead to any secondary phase appearance in a final product.

Distinctly different from conventional ZnS nanowires prepared by catalyst-assisted chemical processes,[10] in which the

* To whom correspondence should be addressed. E-mail: Liu.Baodan@nims.go.jp; baodanliu@gmail.com.
† WPI Center for Materials Nanoarchitectonics (MANA).
‡ Sensor Materials Center.

10.1021/cg9000363 CCC: $40.75
Published on Web 05/12/2009

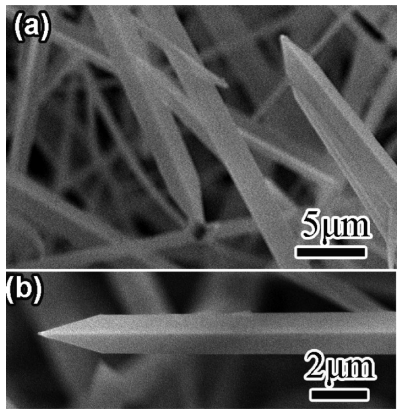

Figure 2. SEM images of bicrystalline ZnS microbelts of a sword-like morphology at low (a) and high (b) magnifications.

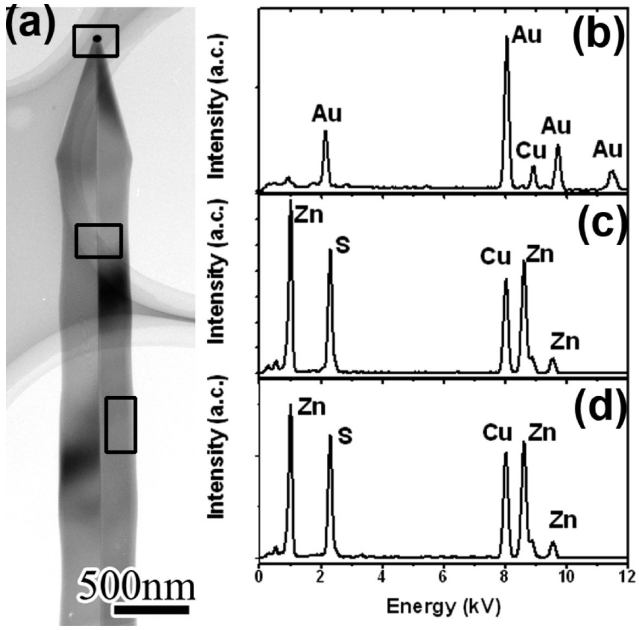

Figure 3. Low-magnification TEM image of a bicrystalline ZnS microbelt starting with the Au particle; (b−d) EDS spectra recorded from the Au tip, twin boundary and the domain edge of the ZnS microbelt shown in (a); the absence of Mn and other impurity peaks verifies the high-purity of the product.

nanostructures show uniform diameter and homogeneous thickness, the present bicrystalline ZnS microbelts exhibit a gradual increase in width starting from the initial Au catalyst position. The structure width stabilizes only after the growth of ~2 μm long segments, as shown in Figure 2b. Different from the conventional vapor−liquid−solid (V−L−S) processes,[11] the Au catalysts here only promote the growth, rather than completely guide it and govern the resultant structure size. Typically, the ZnS belts have an average width larger than 1 μm and a length of up to tens of micrometers. Though the thickness of ZnS microbelts cannot be accurately measured during SEM imaging, they are obviously ultrathin, provided their perfect transparency, as revealed by TEM (Figures 4a and 5a).

It is proposed that MnO_2 additions can locally modify the chemical environment within the reaction cell, although the detailed mechanism is not yet clear and requires further studies. In fact, it was found that formation of bicrystalline ZnS microbelts was particularly dependent on the MnO_2 powders added. Substitution of MnO_2 powder with other additional agents

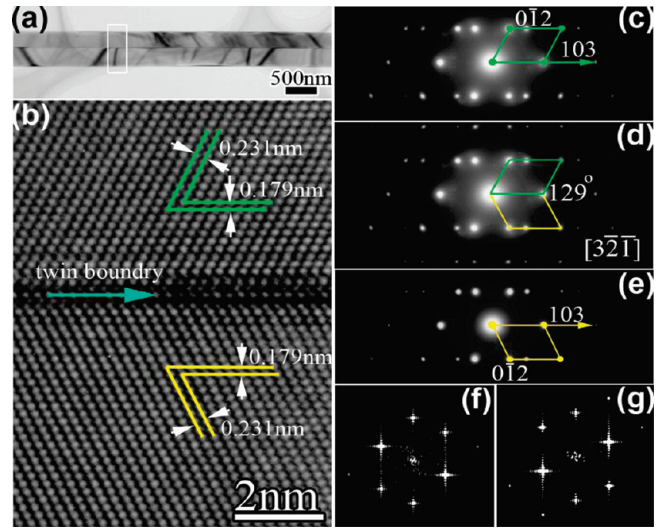

Figure 4. (a) Representative low-magnification TEM image of an individual bicrystalline ZnS microbelt; (b) typical HRTEM lattice image of a bicrystalline ZnS microbelt shown in (a); the *d*-spacings of 0.231 and 0.179 nm between the adjacent lattice fringes correspond to the (0$\bar{1}$2) and (103) planes in wurtzite-type ZnS; the twin structure relationship and the single atomic layer in twin boundary are apparent; (c−e) ED patterns taken along the [3$\bar{2}\bar{1}$] zone axis of wurtzite-type ZnS; (f, g) fast Fourier transform (FFT) patterns derived from the HRTEM image shown in (b); the regular diffraction spots confirm the perfect crystallinity of both mirror domains within the ZnS bicrystal.

or its removal from an original precursor only changed the morphology of ZnS nanostructures (nanorods or nanowires), but no bicrystalline ZnS nanostructures were formed. This result demonstrated that the MnO_2 agent played a certain role in controlling the growth but does not modify the desired belt chemistry. This resembles the formation of ZnS twins with SiO_2 impurities and Sb-induced bicrystal formation in ZnO nanobelts.[4,7]

We did not observe any impurity phases during the XRD measurements. Also, the position of peaks, peculiar to ZnS, was not affected. It was particularly important to understand whether Mn atoms had been penetrated into the ZnS lattice (e.g., substitute for Zn atoms), or arranged themselves at the twin boundary (e.g., to form a local Mn-rich region). Figure 3a presents the TEM image of a representative bicrystalline ZnS microbelt containing a catalyst particle at the tip. Figure 3b−d shows the spatially resolved EDS spectra recorded with the aid of an electron nanoprobe from three different characteristic belt areas. No Mn signal was detected in the belt body. The Zn/S composition ratios were quite similar from one nanostructure to another, suggestive of chemical uniformity. The catalyst particle was composed of pure gold, in line with its standard catalytic action. The EDS analyses on either twin boundary or structure edge revealed slightly Zn-rich compositions with respect to the ZnS (1:1) stoichiometry. No obvious difference in a Zn/S ratio between the twin boundary and edge regions was detected. The absence of Mn signals within the microbelts is in accord with the XRD results.

Though the exact effect of MnO_2 during the formation of the present bicrystalline ZnS microbelts has not yet been understood, it is believed that some novel nanostructures with particular morphologies and unexpected properties can be formed with adding of modifiers in original precursors.[7]

The detailed microstructure of new ZnS bicrystals was understood using a high-resolution TEM and electron diffraction (ED). Figure 4a shows a representative TEM image of an

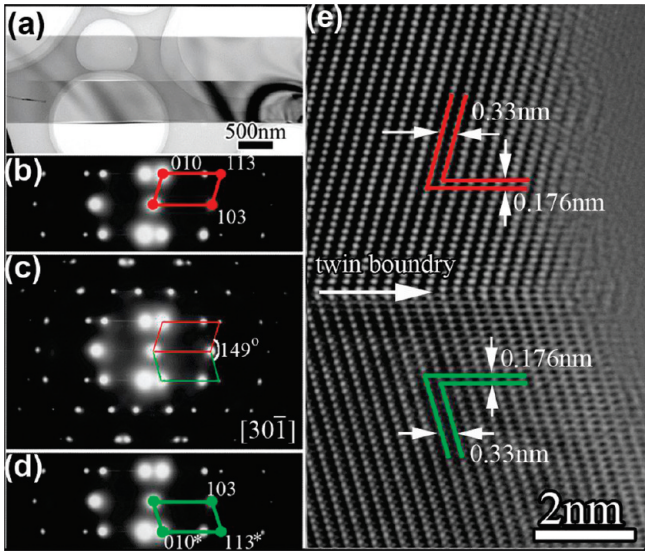

Figure 5. (a) Representative low-magnification TEM image of a bicrystalline ZnS microbelt with another discovered twin structure relationship; (b−d) ED patterns taken along the [30$\bar{1}$] zone axis of wurtzite-type ZnS; (e) ED pattern corresponding to the HRTEM lattice image of a bicrystalline ZnS microbelt; the lattice distances of 0.33 and 0.176 nm between adjacent lattice fringes correspond to the planes of (010) and (103) of a wurtzite-type ZnS.

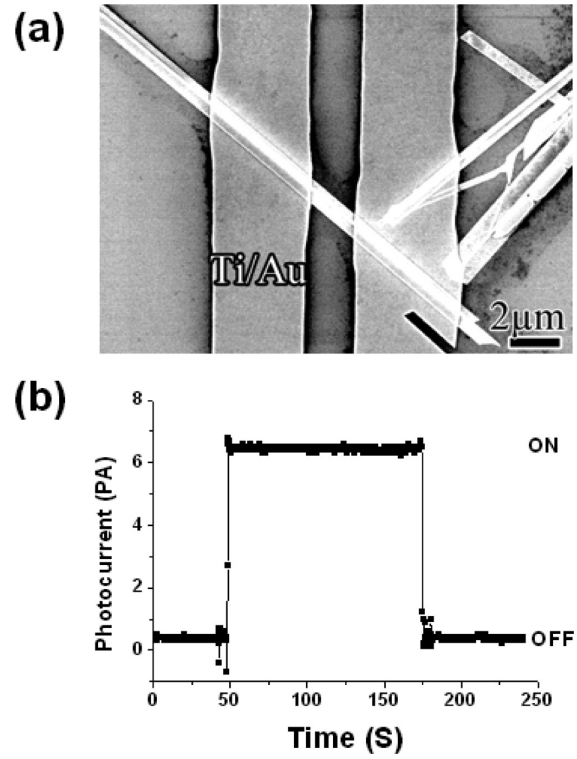

Figure 6. (a) SEM image of the UV sensor made of an individual bicrystalline ZnS microbelt; (b) time response and time-dependent photocurrent recorded from the ZnS UV sensor under the 320 nm UV-light illumination.

individual ultrathin ZnS bicrystalline microbelt with a width of ∼1 μm. The two mirror crystals are tightly joined along the twin boundary. Figure 4b is the HRTEM image of a ZnS microbelt shown in Figure 4a. The corresponding ED pattern is depicted in Figure 4d, that was taken along the [3$\bar{2}\bar{1}$] zone axis. From the HRTEM and ED results, one can clearly verify the symmetrical twin structure relationship within the ZnS microbelts. In order to fully uncover the present twin structure, the ED pattern in Figure 4d was separated into two individual ED patterns, Figure 4c and 4e, each was marked with the corresponding green and red arrows. From the ED patterns (Figure 4c−e), it becomes evident that the bicrystal is composed of the two independent (0$\bar{1}$2) planes, with the (103) plane as the twin plane. From Figure 4b, one can also see that the two well-structured crystals perfectly merge along the twin boundary, and only one single atomic layer of the (103) plane is detected. The measured distances of 0.231 and 0.179 nm between adjacent lattice fringes correspond to the (0$\bar{1}$2) and (103) plane separations in wurtzite-type ZnS with the lattice constants $a = 3.818$ Å, $c = 6.26$ Å (see JCPDS card no. 89-2942). The measured angle of 129° between the two (0$\bar{1}$2) planes is in a good agreement with that calculated from the ED pattern in Figure 4d. The fast Fourier transform (FFT) patterns derived from the HRTEM image in Figure 4b (Figure 4f,g) further verified the perfect crystallinity of each bicrystal domain.

Besides the bicrystals discussed above, we also found other ZnS bicrystals composed of two individual well-crystallized (010) planes symmetrically mirrored by the (103) plane. Analogous bicrystal structure has been observed in sword-like GaN nanowires.[1] GaN has the same hexagonal structure and space group (P_{63mc}) as wurtzite-type ZnS. It is particularly interesting that the different planes, such as (0$\bar{1}$2) and (010), formed the present twinned structures with the same boundary plane (103). Figure 5a is a representative TEM image of the regarded ZnS bicrystal. The HRTEM image and corresponding ED patterns are shown in Figure 5e and Figure 5b−d, respectively. The measured distances of 0.33 and 0.176 nm match well the results of the ED analysis, and approach the data for a bulk ZnS (see JCPDS card no. 89-2942). Similar to the (0$\bar{1}$2)/(103) bicrystals, the (010)/(103) bicrystals also exhibit a single atomic layer at the boundary, as additionally confirmed by the HRTEM image, shown in Figure 5e. In addition, the angle of 149° measured on the HRTEM image is in good agreement with the one in the ED pattern.

Compared with other ZnS nanostructures, for example, nanowires, nanotubes, nanobelts, and nanoribbons,[12−15] the present ultrathin bicrystalline ZnS microbelts exhibit an extremely high aspect ratio, possessing the lengths of up to hundreds of micrometers, but a width of only 1−10 μm. This could be an advantage for their utilization in aspect ratio-related applications such as ultraviolet (UV) sensors. This idea was experimentally checked by us in the course of this work.

Figure 6a shows an UV sensor prepared from a single bicrystalline ZnS microbelt. The preparation of the ZnS UV sensor can be briefly described as follows. First, the ZnS microbelts (ultrasonically dispersed in an ethanol solution) were deposited on a 15 × 15 mm SiO_2/Si substrate. Second, the designed electrode patterns were stamped on the ZnS microbelts using a mask template through an UV irradiation process on the photoresistor layer (this was deposited on the ZnS surface in advance). Lastly, 10-nm Ti and 100-nm Au layers were deposited on the irradiated photoresistor layer and a lift-off process was applied to remove it. The process yielded the bicrystalline ZnS microbelt UV sensor. The distance between the two Ti/Au electrodes in contact with the microbelt was fixed at 2 μm, and a maximum bias voltage of 20 V was applied during the measurements. As plotted in Figure 6b, the ZnS UV-sensor exhibits an ultrafast response to UV light illumination and decent stability under continuous UV irradiation. Though a photocurrent for the present device under 320-nm UV light illumination is in the pA range, thus being lower than for GaN-

and ZnO-based sensors (a photocurrent of the order of $\sim\mu$A,[16,17]), its ultrafast response, high sensitivity, and stability offer a large promise for its further improvement under proper chemical modifications.[18]

Conclusion

In summary, novel bicrystalline structures have been discovered in ZnS microbelts. Formation of the microbelts is totally dependent on MnO_2 additions into starting precursors. HRTEM and ED analyses confirmed that the two newly found ZnS bicrystal structures are composed of $(0\bar{1}2)/(103)$ and $(010)/(103)$ planes with only one atomic layer of the (103) plane as the twin boundary. The method proposed here can be widen to grow other prospective nanostructures with tunable morphologies for specific applications. The presently achieved ultrahigh bicrystal aspect ratio offers their prominent use in nanoscaled UV sensors and other optoelectronic nanodevices.

Acknowledgment. The authors would like to thank Drs. A. Nukui, C. Y. Zhi, X. S. Fang, and C. Li of the National Institute for Materials Science (NIMS) in Japan for a technical support, kind help, and valuable discussions in the course of this work. B.L. particularly appreciates the kind assistance of Drs. R. Lee, S. Hara, and H. Sugaya (Nanofoundary, NIMS) during fabrication of ZnS nanodevices. The work was partially supported by the World Premier International Center for Materials Nanoarchitectonics (MANA) of the National Institute for Materials Science (NIMS), Tsukuba, Japan.

Supporting Information Available: A detailed experimental setup for the ZnS microbelt growth (Figure SI-1). This material is available free of charge via the Internet at http://pubs.acs.org.

References

(1) Liu, B. D.; Bando, Y.; Tang, C. C.; Xu, F. F.; Hu, J. Q.; Golberg, D. *J. Phys. Chem. B* **2005**, *109*, 17082.
(2) Xu, C.; Chun, J.; Rho, K. *Appl. Phys. Lett.* **2006**, *89*, 93117–1.
(3) Spearot, D. E.; Jacob, K. I.; McDowell, D. L. *J. Eng. Mater. Technol.* **2005**, *127*, 374.
(4) Zou, K.; Qi, X. Y.; Duan, X. F.; Zhou, S. M.; Zhang, X. H. *Appl. Phys. Lett.* **2005**, *86*, 013103.
(5) Weber, C.; Klushin, A. M.; Beuven, S.; van der Hart, A.; Kohlstedt, H.; Semerad, R.; Prusseit, W. *IEEE Trans. Appl. Supercond.* **1999**, *9*, 4162.
(6) Hao, Y.; Meng, G.; Wang, Z. L.; Ye, C. H.; Zhang, L. D. *Nano. Lett.* **2006**, *6*, 1650.
(7) Meng, X. M.; Jiang, Y.; Liu, J.; Lee, C. S.; Beiio, I.; Lee, S. T. *Appl. Phys. Lett.* **2003**, *83*, 2244.
(8) Liang, C. H.; Shimizu, Y.; Sasaki, T.; Umehara, H.; Koshizaki, N. *J. Phys. Chem. B* **2004**, *108*, 9278.
(9) Zhang, Z.; Wang, J.; Yuan, H.; Gao, Y.; Liu, D.; Song, L.; Xiang, Y.; Zhao, X.; Liu, L.; Luo, S.; Dou, X.; Mou, S.; Zhou, W.; Xie, S. *J. Phys. Chem. B* **2005**, *109*, 18352.
(10) Lin, M.; Sudhiranjan, T.; Boothroyd, C.; Loh, K. P. *Chem. Phys. Lett.* **2004**, *400*, 175.
(11) Wagner, R. S.; Ellis, W. C. *Appl. Phys. Lett.* **1964**, *4*, 89.
(12) Ye, C. H.; Fang, X. S.; Li, G. H.; Zhang, L. D. *Appl. Phys. Lett.* **2004**, *85*, 3035.
(13) Fang, X. S.; Bando, Y.; Shen, G. Z.; Ye, C. H.; Gautam, U. K.; Costa, P. M. F. J.; Zhi, C. Y.; Tang, C. C.; Golberg, D. *Adv. Mater.* **2007**, *19*, 2593.
(14) Shen, G. Z.; Bando, Y.; Hu, J. Q.; Golberg, D. *Appl. Phys. Lett.* **2007**, *90*, 123101.
(15) Yin, L. W.; Bando, Y.; Zhan, J. H.; Li, M. S.; Golberg, D. *Adv. Mater.* **2005**, *17*, 1972.
(16) Lee, J. W.; Moon, K. J.; Ham, M. H.; Myoung, J. M. *Solid State Commun.* **2008**, *148*, 194.
(17) Soci, C.; Xiang, B.; Dayeh, S. A.; Aplin, D. P. R.; Park, J.; Bao, X. Y.; Lo, Y. H.; Wang, D. *Nano Lett.* **2007**, *7*, 1003.
(18) He, J. H.; Lin, Y. H.; McConney, M. E.; Tsukruk, V. V.; Wang, Z. L. *J. Appl. Phys.* **2007**, *102*, 084303.

CG9000363